Analysis of Cross Modulation in W-CDMA Receivers

Vladimir Aparin† and Lawrence E. Larson‡

† QUALCOMM Inc., San Diego, CA 92121
‡ University of California in San Diego, La Jolla, CA 92093

Abstract **— Cross modulation distortion (XMD) of a narrow- and wide-band jammers in W-CDMA mobile receivers is analyzed using statistical methods and a novel HPSK signal model. Statistical properties of HPSK signals are compared to those of QPSK and OQPSK signals and their effect on XMD is explained. The derived closed-form expressions for XMD are confirmed by the measured data.**

Index Terms **— Code division multiaccess, cross modulation distortion, nonlinear circuits, spectral analysis, statistics.**

I. Introduction

Mobile wireless receivers operate in a jamming environment due to coexistence of many wireless standards. Besides external jammers, mobile CDMA stations are subject to interference from its own transmitter (TX) whose signal leaks through the antenna duplexer to the receiver input as shown in Fig. 1. The LNA nonlinearities transfer the modulation from the TX leakage to an external jammer resulting in cross modulation distortion (XMD) which contaminates the channels adjacent to the jammer degrading the receiver sensitivity for these channels. In W-CDMA systems, the external jammer can be narrow- or wide-band. The narrow-band jammer is a GSM signal or its harmonic [2] or an LO leakage in a zero-IF receiver [3]. The wide-band jammer is a strong W-CDMA signal transmitted by a competitor base station [4].

The linearity of CDMA LNAs is typically specified as the input-referred 3rd-order intercept point (IIP_3) because intermodulation distortion (IMD) is easier to simulate and measure than XMD. However, in contrast to IMD, XMD depends on the statistical properties of the modulated signal (TX leakage). Therefore, a correlation formula between XMD and IIP_3 is required for correct system analysis and specification. Such a formula for cdmaOne (IS-95) systems has been derived in [1].

Here we derive closed-form expressions for XMD of narrow- and wide-band jammers in W-CDMA mobile receivers based on the proposed model of a Hybrid Phase Shift Keying (HPSK) signal. Statistical properties of HPSK and O/QPSK signals are compared and their effect on XMD is explained. The theoretical results are confirmed by the measured data.

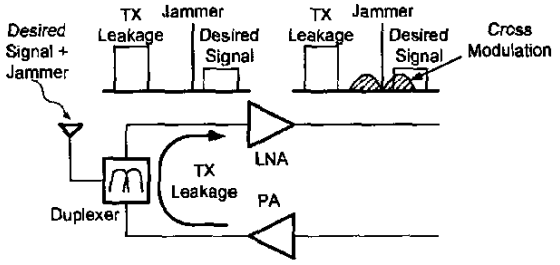

Fig. 1. Cross modulation in a CDMA transceiver.

II. HPSK Signal Model

W-CDMA uplink modulators use HPSK spreading [5]. The HPSK signal model for single I and Q channels of equal power can be obtained by following the derivations in [1]. Using the same assumptions that the I and Q binary sequences are infinitely long and the baseband filters are ideal low-pass filters with a cut-off frequency of half the spreading rate, the transmitted signal can be described as:

$$c(t) = i(t) + q(t) \tag{1a}$$

where

$$i(t) = \cos(\omega_c t + \theta) I(t), \tag{1b}$$

$$q(t) = \sin(\omega_c t + \theta) Q(t), \tag{1c}$$

$$I(t) = \sum_{k=-\infty}^{\infty} i_k \,\mathrm{sinc}(Bt + \phi/\pi - k), \tag{1d}$$

$$Q(t) = \sum_{k=-\infty}^{\infty} q_k \,\mathrm{sinc}(Bt + \phi/\pi - k), \tag{1e}$$

i_k and q_k are uncorrelated random numbers taking values of ± 1 with equal probability, B is the spreading rate, ω_c is the angular frequency of the carriers, θ and ϕ are independent random phases uniformly distributed in $(0, 2\pi)$, and $sinc(z) = sin(\pi z)/(\pi z)$. Due to the randomness and zero crosscorrelation of θ and ϕ, the statistical properties of $i(t)$ and $q(t)$ are time-independent. Therefore, t will be set to zero in further derivations to simplify them.

The possible transitions between the sequential chips in HPSK are shown in Fig. 2 [5]. Mathematically, the rela-

0-7803-8331-1/04/$20.00 © 2004 IEEE

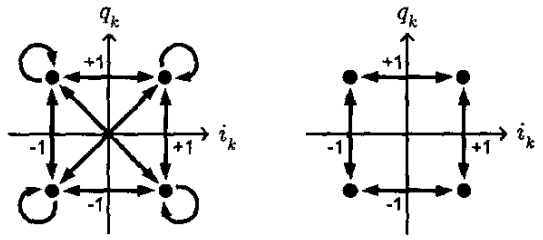

(a) From odd chip to even chip (b) From even chip to odd chip

Fig. 2. Transitions in HPSK constellation.

tionship between these chips can be described as:

$$i_{2k+1} = i_{2k} r_{2k}, \tag{2a}$$

$$q_{2k+1} = -q_{2k} r_{2k}, \tag{2b}$$

where r_k is a random number independent of i_k and q_k and taking values of ± 1 with equal probability.

Some of the statistical properties of i_k and q_k in the HPSK and O/QPSK spreadings are compared in Table I where $E\{\}$ is the statistical average (or expectation) and δ_{kl} is the Kronecker delta. As can be seen, the moments of i_k and q_k are the same for the compared spreadings except for the higher order even joint moments ($E\{i_k i_l q_m q_n\}$, etc.) With a large number of transmitted channels, i_k and q_k become normally distributed according to the Central Limit Theorem and, thus, the resulting signal behaves as a Band-Pass Gaussian Noise (BPGN) regardless of the spreading.

TABLE I

STATISTICAL PROPERTIES OF i_k AND q_k

Moment	O/QPSK	HPSK
$E\{i_k^n\}$, $E\{q_k^n\}$	0, n is odd 1, n is even	0, n is odd 1, n is even
$E\{i_k i_l\}$, $E\{q_k q_l\}$	δ_{kl}	δ_{kl}
$E\{i_k q_l\}$	0	0
$E\{i_k i_l i_m i_n\}$, $E\{q_k q_l q_m q_n\}$	$\delta_{kl}\delta_{mn} + \delta_{km}\delta_{ln}$ $+\delta_{kn}\delta_{lm}$ $-2\delta_{kl}\delta_{km}\delta_{kn}$	$\delta_{kl}\delta_{mn} + \delta_{km}\delta_{ln}$ $+\delta_{kn}\delta_{lm}$ $-2\delta_{kl}\delta_{km}\delta_{kn}$
$E\{i_k i_l q_m q_n\}$	$\delta_{kl}\delta_{mn}$	$\delta_{kl}\delta_{mn}$ $-2\delta_{km}\delta_{ln}\delta_{k-1,l}\big\vert_{\text{odd } k}$ $-2\delta_{km}\delta_{ln}\delta_{k+1,l}\big\vert_{\text{even } k}$
All odd-order	0	0

III. Analysis of Cross Modulation Distortion

A. Narrow-Band Jammer

Let the transfer function of a receiver circuit such as an LNA be described by the following power series

$$y(t) = \sum_{n=1}^{\infty} y_n(t) \qquad \text{with} \qquad y_n(t) = a_n x^n(t) \tag{3}$$

where $y(t)$ is the output signal, $x(t)$ is the input signal and a_n's are the expansion coefficients. Let

$$x(t) = j(t) + l(t) \tag{4}$$

where $j(t) = V_j \cos(\omega_j t + \psi)$ is a continuous-wave (CW) jammer with an amplitude V_j and a random phase ψ uniformly distributed in $(0, 2\pi)$, and $l(t) = V_{c,\text{rms}} c(t)$ is a TX leakage with a root-mean-square voltage $V_{c,\text{rms}}$. The TX signal is assumed to carry single I and Q channels of equal power.

After passing through the circuit, the jammer spectrum is widened by XMD generated by the odd-order nonlinear terms in (3). Terms of order higher than three will be neglected here since most receiver front ends operate far below their 1dB gain compression. The autocorrelation function of the 3rd-order term in (3) is

$$\begin{aligned} R_{y_3}(\tau) &= E\{y_3(0) y_3(\tau)\} \\ &= a_3^2 E\left\{[j(0) + l(0)]^3 [j(\tau) + l(\tau)]^3\right\}. \end{aligned} \tag{5}$$

After expanding the argument of $E\{\}$ in (5), some of its terms will be zero due to the zero means of $j(t)$ and $l(t)$ and their zero crosscorrelation. Keeping only the nonzero terms, we get

$$\begin{aligned} R_{y_3}(\tau) = a_3^2 E\{&j^3 j_\tau^3 + l^3 l_\tau^3 + 3j^3 j_\tau l_\tau^2 + 3j j_\tau^3 l^2 + 3j^2 l l_\tau^3 \\ &+ 3j_\tau^2 l^3 l_\tau + 9 j^2 j_\tau^2 l l_\tau + 9 j j_\tau l^2 l_\tau^2\} \end{aligned} \tag{6}$$

where j, l, j_τ and l_τ denote $j(0)$, $l(0)$, $j(\tau)$ and $l(\tau)$ respectively. Among the averaged terms in (6), only $9 j j_\tau l^2 l_\tau^2$ includes the jammer XMD. Its average is

$$\begin{aligned} E\{9 j j_\tau l^2 l_\tau^2\} &= \frac{9 V_j^2 V_{c,\text{rms}}^4}{2} \cos(\omega_j \tau) E\{c^2(0) c^2(\tau)\} \\ &= 9 P_j P_c^2 \cos(\omega_j \tau) E\{i^2 i_\tau^2 + q^2 q_\tau^2 + i^2 q_\tau^2 \\ &\qquad + i_\tau^2 q^2 + 4 i i_\tau q q_\tau\} \end{aligned} \tag{7}$$

where $P_j = V_j^2/2$ and $P_c = V_{c,\text{rms}}^2$ are the jammer and TX leakage input powers respectively. We omitted the terms with the odd number of $i(t)$ or $q(t)$ under $E\{\}$ in the last part of (7) because their averages are zero. Among the remaining terms, only the first four contribute to the distortion centered at ω_j. It can be shown that $E\{i^2 i_\tau^2\} = E\{q^2 q_\tau^2\}$ and $E\{i^2 q_\tau^2\} = E\{i_\tau^2 q^2\}$.

The averages $E\{i^2 i_\tau^2\}$ and $E\{i^2 q_\tau^2\}$ can be expanded further as follows

$$\begin{aligned} E\{i^2 i_\tau^2\} &= E_\theta\{\cos^2(\theta) \cos^2(\omega_c \tau + \theta)\} E_{i,\phi}\{I^2 I_\tau^2\} \\ &= \left[\frac{1}{4} + \frac{\cos(2\omega_c \tau)}{8}\right] E_{i,\phi}\{I^2 I_\tau^2\}, \end{aligned} \tag{8}$$

$$E\{i^2 q_\tau^2\} = \left[\frac{1}{4} - \frac{\cos(2\omega_c \tau)}{8}\right] E_{i,q,\phi}\{I^2 Q_\tau^2\}, \quad (9)$$

where I, Q, I_τ and Q_τ denote $I(0)$, $Q(0)$, $I(\tau)$ and $Q(\tau)$ respectively and the subscript of E indicates the variable over which the averaging is performed.

To find $E_{i,\phi}\{I^2 I_\tau^2\}$, we first take an average over i_k:

$$E_i\{I^2 I_\tau^2\} = \sum_{k,l,m,n} E\{i_k i_l i_m i_n\} \operatorname{sinc}(\phi/\pi - k) \cdot \operatorname{sinc}(\phi/\pi - l) \operatorname{sinc}(B\tau + \phi/\pi - m) \cdot \operatorname{sinc}(B\tau + \phi/\pi - n). \quad (10)$$

Using the result for $E\{i_k i_l i_m i_n\}$ from Table I, we get

$$E_i\{I^2 I_\tau^2\} = s(2,0)s(0,2) + 2s(1,1)^2 - 2s(2,2) \quad (11)$$

where

$$s(\alpha,\beta) = \sum_{k=-\infty}^{\infty} \operatorname{sinc}^\alpha(\phi/\pi - k) \operatorname{sinc}^\beta(B\tau + \phi/\pi - k). \quad (12)$$

Evaluating (11) and averaging it over ϕ, we get

$$E_{i,\phi}\{I^2 I_\tau^2\} = 1 + 2\operatorname{sinc}^2(B\tau) - 2\frac{1 - \operatorname{sinc}(2B\tau)}{(\pi B\tau)^2}. \quad (13)$$

This result is also valid for O/QPSK signals.

The average $E_{i,q}\{I^2 Q_\tau^2\}$ in (9) can be expanded as

$$E_{i,q}\{I^2 Q_\tau^2\} = \sum_{k,l,m,n} E\{i_k i_l q_m q_n\} \operatorname{sinc}(\phi/\pi - k) \cdot \operatorname{sinc}(\phi/\pi - l) \operatorname{sinc}(B\tau + \phi/\pi - m) \cdot \operatorname{sinc}(B\tau + \phi/\pi - n). \quad (14)$$

Using the result for $E\{i_k i_l q_m q_n\}$ from Table I, we get

$$E_{i,q}\{I^2 Q_\tau^2\} = 1 - 4\sum_{k=-\infty}^{\infty} \operatorname{sinc}(\phi/\pi - 2k) \cdot \operatorname{sinc}(\phi/\pi - 2k - 1) \cdot \operatorname{sinc}(B\tau + \phi/\pi - 2k) \cdot \operatorname{sinc}(B\tau + \phi/\pi - 2k - 1). \quad (15)$$

Evaluation of (15) followed by averaging over ϕ gives

$$E_{i,q,\phi}\{I^2 Q_\tau^2\} = 1 - \frac{2\operatorname{sinc}(2B\tau)}{\pi^2(1 - B^2\tau^2)}. \quad (16)$$

For O/QPSK signals, $E_{i,q,\phi}\{I^2 Q_\tau^2\} = 1$.

After substituting (13) and (16) into (8) and (9) respectively, and the latter into (7), we find that the first term in (13) and (16) and the second term in brackets of (8) and (9) do not contribute to XMD. Omitting these terms and multiplying (7) by a_3^2, we get the following autocorrelation function of the XMD

$$R_{\mathrm{XMD}}(\tau) = 9a_3^2 P_j P_c^2 \cos(\omega_j \tau)\left[\operatorname{sinc}^2(B\tau) - \frac{1 - \operatorname{sinc}(2B\tau)}{(\pi B\tau)^2} - \frac{\operatorname{sinc}(2B\tau)}{\pi^2(1 - B^2\tau^2)}\right]. \quad (17)$$

The 3rd-order expansion coefficient a_3 can be expressed as a function of IIP_3 as

$$a_3^2 = 4G/(9 \cdot \mathrm{IIP}_3^2) \quad (18)$$

where G is the power gain of the circuit. Substituting (18) into (17) and taking the Fourier transform of (17), the following two-sided power spectral density (PSD) function of the XMD can be obtained:

$$S_{\mathrm{XMD}}(u) = \frac{2GP_jP_c^2}{B \cdot \mathrm{IIP}_3^2}\left[|u| - u^2 - \frac{\sin^2(\pi u)}{\pi^2}\right] \quad (19)$$

for $|u| < 1$ where $u = (|\omega| - \omega_j)/(2\pi B)$.

It can be shown that, if the TX leakage is a QPSK or OQPSK signal, the term in brackets of (19) is $|u| - u^2$. If the TX leakage is a multi-channel signal, it behaves as BPGN and the mentioned term is $1 - |u|$.

B. Wide-Band Jammer

Assuming that the jammer has the same bandwidth as the TX leakage, its XMD is described by the autocorrelation function (17) with an extra multiplicand $\operatorname{sinc}(B\tau)$. The Fourier transform of this autocorrelation function gives the following PSD:

$$S_{\mathrm{XMD}}(v) = \frac{3GP_jP_c^2}{4B \cdot \mathrm{IIP}_3^2}\left[3|v|(1 - |v|)^2 - 2\frac{1 - |v| - |v|\operatorname{sinc}(3v)}{\pi^2}\right] \quad (20)$$

for $1/3 < |v| < 1$ where $v = (|\omega| - \omega_j)/(3\pi B)$. It can be shown that, for a QPSK or OQPSK TX signal, the term in brackets of (20) is $3|v|(1 - |v|)^2$ and, for a multi-channel TX signal or BPGN, that term is $3(1 - |v|)^2$

The statistical properties of the jammer do not affect its XMD but affect its own spectral regrowth which adds to the total distortion centered around ω_j. In most cases, the XMD is dominant.

IV. Measured Results

The theoretical and measured single-sided XMD spectra[1] of a CW jammer for different TX spreadings are plotted in

[1]The theoretical single-sided PSD was computed as $2S_{\mathrm{XMD}}$.

Fig. 3 and 4 respectively for an amplifier with $G = 14.5$dB and $\mathrm{IIP}_3 = -6.7$dBm ($P_c = P_j = -25$dBm). The spreading rate of the TX leakage was selected $B = 1.2288$Mcps for convenience. Fig. 5 and 6 show the theoretical and measured single-sided XMD spectra of a wide-band jammer (a QPSK signal) for the same amplifier ($P_j = -35$dBm, $P_c = -25$dBm). In both cases, the theoretical results agree well with the measured data.

V. Conclusion

We have proposed a new model of HPSK signals and used it to derive simple expressions for XMD in W-CDMA receivers. The derivations show that XMD is affected by the 4th-order joint moments of the I and Q bits. These moments are different between O/QPSK and HPSK spreadings resulting in their different distortions. The measured data confirmed the analytical results proving the theory. The derived expressions can be used in W-CDMA system analysis and specification.

References

[1] V. Aparin and L. E. Larson, "Analysis and reduction of cross modulation distortion in CDMA receivers," *IEEE Trans. Microwave Theory Tech.*, vol. 51, no. 5, pp. 1591-1602, May 2003.

[2] *Signal characteristics for narrow band blocker for UMTS 1800/1900*, R4-011227, 3GPP TSG-RAN WG4 Meeting #19, Sept. 2001.

[3] S. K. Reynolds *et al.*, "A direct conversion receiver IC for WCDMA mobile systems," *IBM J. Res. & Dev.*, vol. 47, no. 2/3, pp. 337-353, March/May 2003.

[4] G. Povey *et al.*, "WCDMA inter-operator interference and 'dead zones'," *5th Europ. Pers. Mobile Comm. Conf.*, pp. 560-564, Glasgow, Apr. 2003.

[5] *HPSK Spreading for 3G*, Agilent App. Note 1335.

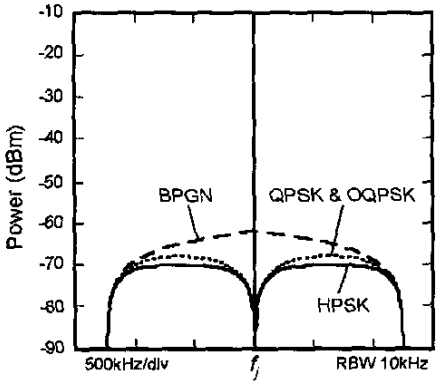

Fig. 3. Theoretical single-sided XMD spectra of a CW jammer.

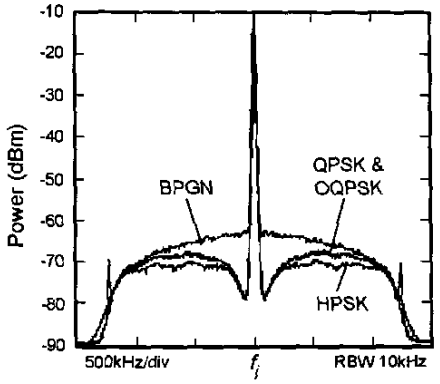

Fig. 4. Measured single-sided XMD spectra of a CW jammer.

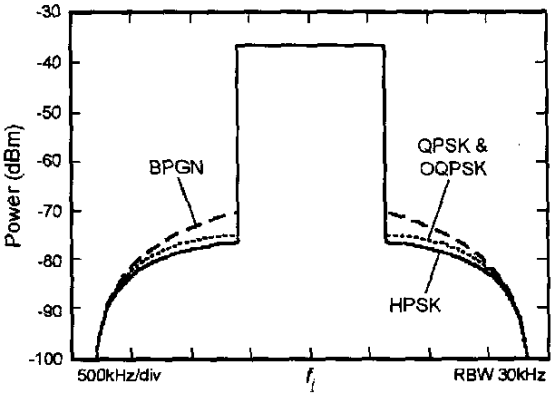

Fig. 5. Theoretical single-sided XMD spectra of a wide-band jammer.

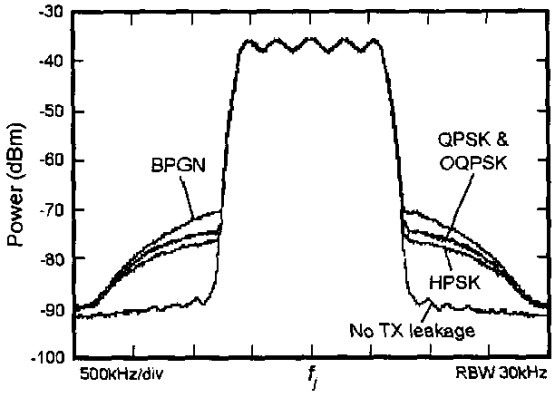

Fig. 6. Measured single-sided XMD spectra of a wide-band jammer.